THE JOURNAL OF PHYSICAL CHEMISTRY C

pubs.acs.org/JPCC

Article

Growth Dynamics and Processes Governing the Stability of Electrodeposited Size-Controlled Cubic Cu Catalysts

Published as part of The Journal of Physical Chemistry virtual special issue "Metal Clusters, Nanoparticles, and the Physical Chemistry of Catalysis".

Philipp Grosse, Aram Yoon, Clara Rettenmaier, See Wee Chee, and Beatriz Roldan Cuenya*

Cite This: *J. Phys. Chem. C* 2020, 124, 26908−26915

Read Online

ACCESS | Metrics & More | Article Recommendations | Supporting Information

ABSTRACT: The renewable energy-powered conversion of industrially generated CO_2 into useful chemicals and fuels is considered a promising technology for the sustainable development of our modern society. The electrochemical reduction of CO_2 (CO_2RR) is one of the possible conversion processes that can be employed to close the artificial carbon cycle, mimicking nature's photosynthesis. Nevertheless, to enable green catalytic processes, selectivity for the desired products must be achieved. In the case of CO_2RR, the selectivity is strongly dependent on the electrocatalyst structure. Here, we explore the phase space of synthesis parameters required for the electrodeposition of Cu cubes with {100} facets on glassy carbon substrates and elucidate their influence on the size, shape, coverage, and uniformity of the cubes. We found that the concentration of Cl^- ions in solution controls the cube size, shape, and coverage, whereas the ratio of the reduction versus oxidation time and number of cycles in the alternating potential electrodeposition protocol can be used to further tune the cube size. Cyclic voltammetry experiments were complemented with *in situ* electrochemical scanning electron microscopy to follow the growth dynamics and *ex situ* transmission electron microscopy and electron diffraction. Our results indicate that the cube growth starts from nuclei formed during the first cycle, followed by a layered deposition and partial dissolution of new material in subsequent cycles.

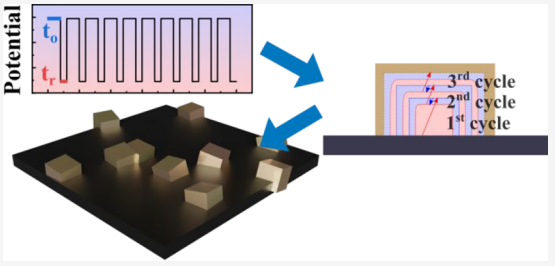

INTRODUCTION

With increasing awareness of the need to mitigate climate change, research into renewable and sustainable energy technologies has intensified over the past decade. Conversion reactions that turn simple and abundant base molecules,[1] such as CO_2, H_2O, and N_2, into valuable, industrially relevant chemicals, have been the focus of these research efforts. This includes the electrochemical CO_2 reduction (CO_2RR) to hydrocarbons and fuels[2,3] and the oxygen and hydrogen evolution reactions (OER and HER)[4,5] for the generation of green hydrogen and fuel cell applications. Copper-based materials have attracted significant interest due to their promise as catalysts for CO_2RR conversion to ethylene and ethanol,[2] the electrochemical nitrate reduction to ammonia,[6] and photocatalytic applications due to the favorable bandgap of Cu_2O[7] or the supercapacitative features of Cu_2O for energy storage.[8]

In CO_2RR, copper has the unique ability of reducing CO_2 into hydrocarbons in significant yields.[2] Several properties of catalysts derived from copper are known to impact the catalytic activity and selectivity, such as their morphology and surface structure (roughness,[9] grain boundaries,[10,11] crystalline facets,[12−17] and defects[18−20]) and chemical state[21−26] (subsurface oxygen and Cu(I) species[27−36]). In particular, nanostructured Cu catalysts are interesting not only because of their high surface-to-volume ratio, which leads to an increased catalytic activity as compared to bulk polycrystalline Cu electrodes, but also because their selectivity is strongly dependent on the NP size and shape.

It is known from single-crystal studies that Cu{100} has superior selectivity toward ethylene and ethanol production vs other crystalline orientations.[37] On the basis of theoretical calculations, it has been hypothesized that the bonding distance of two or more adsorbed CO molecules on the {100} surface favors the C−C coupling and thus influences the desired selectivity toward C2+ products.[38−40] Hence, cubic nanoparticles exclusively made of {100} facets have arisen significant interest for future industrial applications.[12]

There are various approaches to create size- and shape-controlled particles for use as electrocatalysts, such as colloidal synthesis,[41] laser ablation,[42] sol−gel,[43,44] chemical vapor deposition,[45] and electrochemical synthesis methods.[28,46]

Received: October 7, 2020
Revised: November 13, 2020
Published: November 26, 2020

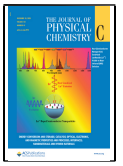

https://dx.doi.org/10.1021/acs.jpcc.0c09105
J. Phys. Chem. C 2020, 124, 26908−26915

Among these techniques, the electrochemical deposition of copper particles has the following advantages: (1) the catalysts are directly deposited on the working electrode, which ensures good adhesion; (2) the catalyst shape and hence their surface exposure are easily tuned through the addition of halide ions to the copper precursor solution;[29,47] and (3) the use of surfactant ligands to achieve shape control is avoided, which otherwise requires additional chemical treatments to remove them to achieve a pristine catalyst surface. Moreover, the presence of halide ions in the electrolyte may act as another factor that can be used to tune the catalytic selectivity.[48] However, the phase space of synthesis parameters that needs to be explored to obtain catalysts with narrow size and shape distributions is large. These include, the optimum Cu precursor salt, optimum Cu concentration in the electrolyte, optimum Cl^- concentration (and how this affects the resulting average particle size), the potential range employed, and the duration of the electrodeposition as well as the pH of the electrolyte.

Recently, we reported a protocol that achieves the direct growth of copper particles from solution onto carbon-based supports with a narrow shape distribution using alternating potentials, where the potential window is tuned such that only the noncubic particles dissolve.[47] In this present study, we discuss the role of other important synthesis parameters namely, the Cu/Cl^- concentration, the number of cycles, speed, potential, and how they affect the final electrocatalyst shape and size distribution. In particular, we found that the Cl^- concentration[49] had the most drastic effect on the catalyst size distribution and coverage. We further studied the dynamic morphology of the electrodeposited Cu particles via *in situ* electrochemical scanning electron microscopy (SEM) to gain insight into the details of the growth pathways. Our results show that nuclei for the cubes are formed during the first pulse electrochemical cycle, which progressively grow into cubes in the subsequent alternating reductive−oxidative cycles as new material is deposited and partially removed.

EXPERIMENTAL METHODS

Synthesis. A mixture of 5 mM copper sulfate−pentahydrate ($CuSO_4 \cdot 5H_2O$) (Sigma-Aldrich, 99.7−100.5%) and 5, 10, 30, or 50 mM potassium chloride (KCl) (Sigma-Aldrich, 99%) has been used as electrochemical deposition solution. The synthesis was performed in a three-electrode configuration, equipped with an Ag/AgCl (sat.) reference electrode (Gaoss union), a Pt counter electrode, and polished glassy carbon (vitreous) plates (SPI) as working electrodes. Electrochemical cycling between an anodic (+0.0 V vs Ag/AgCl) and a cathodic potential (−0.5 V vs Ag/AgCl) within a total of 10 cycles results in the electrodeposition of size- and shape-controlled Cu cubes. Initially, a potential of −0.5 V vs Ag/AgCl was held for 8 s followed by a potential jump to +0.0 V vs Ag/AgCl for 4 s. The cyclic voltammetry is completed by returning to the initial potential

Morphological Characterization. The samples were characterized by using a 200 kV Talos transmission electron microscope (TEM) from Thermo Fisher. The *in situ* electrochemical scanning electron microscopy (SEM) experiments were performed in an 30 kV Apreo scanning electron microscope from Thermo Fischer using a customized liquid flow cell setup from Hummingbird Scientific with dedicated Ag/AgCl (3 M) reference and Pt counter electrodes. The electrodeposition studies were performed by using liquid cell chips from Hummingbird Scientific that are patterned with a carbon working electrode. The image sequences following the electrodeposition process were acquired by using the transmission electron detector.

For each precursor solution containing a defined ratio of Cu to Cl, three samples were produced, and the microscopy measurements were conducted in several different locations of the sample to check the homogeneity of the electrodeposition process. An automatic particle detection and counting algorithm from the Gwyddion software was utilized. The respective SEM size distributions were calculated based on data obtained from at least three different positions on the sample. The interconnected cubes are counted as individual cubes for statistics, whereas the size distributions are obtained only from isolated cubes. The distributions were fitted with a Gaussian curve to yield the average sizes displayed in Tables 1 and 2.

Table 1. Size Distribution of the Different Electrodeposited Cu Samples with Varying Precursor Concentrations Ranging from 5 to 50 mM Cu-to-Cl Ratio Fitted by a Gaussian Peak Shape[a]

$CuSO_4$ conc (mM)	KCl conc (mM)	Cu:Cl ratio	size (nm)	no. of cubes/cm^2	Cu surface area (cm^2)
5	0	1:0	596 ± 47	9.0×10^6	1.6×10^{-1}
5	5	1:1	291 ± 32	1.6×10^8	6.6×10^{-1}
5	10	1:2	125 ± 5	9.1×10^8	7.1×10^{-1}
5	30	1:6	44 ± 4	1.8×10^{10}	17.3×10^{-1}
5	50	1:10	39 ± 3	5.5×10^9	4.2×10^{-1}
50	5	10:1	87 ± 7[b]		

[a]The times t_r and t_o were kept at 4 and 8 s, respectively, and the number of cycles was kept constant and set to 10 cycles. The column (no. of cubes/cm^2) indicates the number of Cu cubes detected per cm^2 of the support, while the last column describes the specific Cu surface area per cm^2 of sample. [b]Size of the cubes in the branched structures.

Table 2. Size Distribution and Specific Cu-Cube Area Estimation Results Normalized to 1 cm^2 as a Function of the Electrochemical Protocol Applied (Fitted by the Gaussian Peak Shape)[a]

t_r (s)	t_o (s)	size (nm)	no. of cubes/cm^2	Cu surface area (cm^2)
4	8	291 ± 32	6.6×10^8	27.9×10^{-1}
4	4	130 ± 3	21.9×10^8	18.5×10^{-1}
8	4	340 ± 10	1.6×10^8	9.6×10^{-1}

[a]Here the concentration was kept at 5 mM for KCl and $CuSO_4$ (1:1), and only the times are altered. The column (no. of cubes/cm^2) indicates the number of Cu cubes detected per cm^2 of the support, while the last column describes the specific Cu surface area per cm^2 of sample.

RESULTS AND DISCUSSION

Effect of Different Synthesis Parameters on Catalyst Morphology. In addition to achieving shape selection,[23] here we attempt to explore the parameters and conditions required to grow uniformly dispersed, size-controlled Cu cubes from a solution of $CuSO_4$ and KCl.[23] Although it was previously established that the presence of Cl^- ions in solution is crucial for the electrochemical growth of the Cu cubes,[47] no information was yet available on how to simultaneously tailor their size, distribution, and coverage on the support.

https://dx.doi.org/10.1021/acs.jpcc.0c09105
J. Phys. Chem. C 2020, 124, 26908−26915

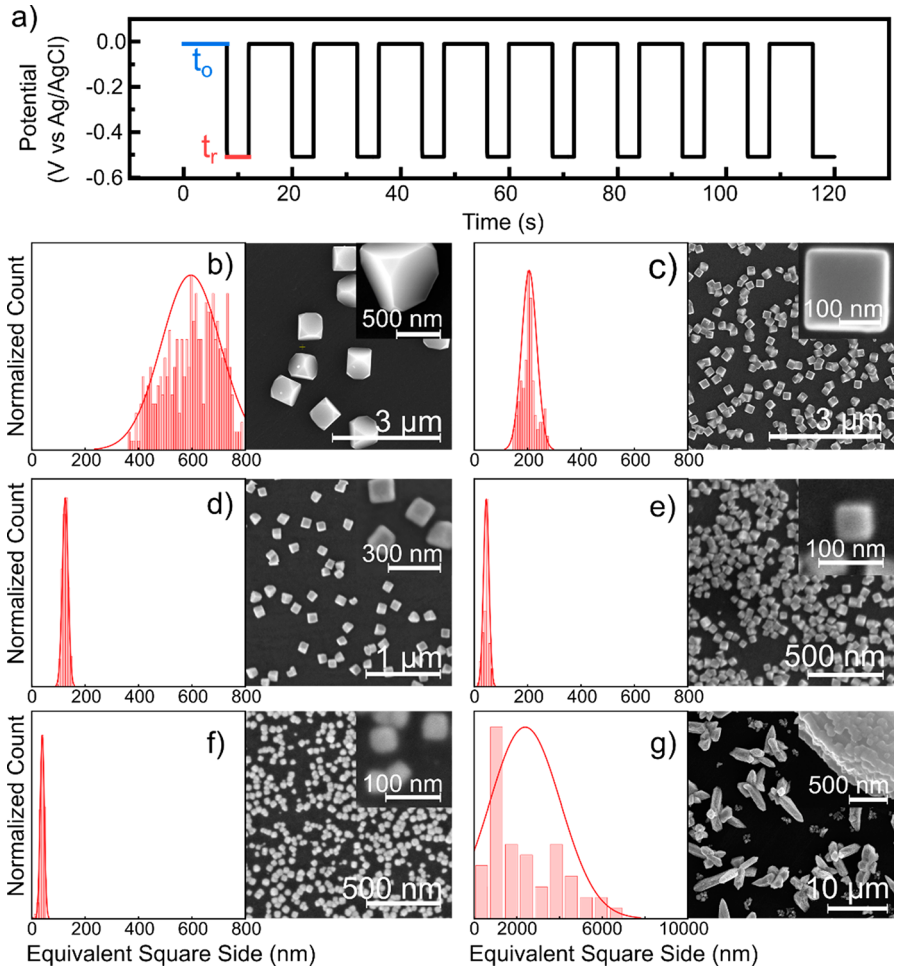

Figure 1. (a) Synthesis protocol with alternating potentials of 0 and −0.5 V vs Ag/AgCl and fixed oxidizing (t_o) and reductive (t_r) time length (t_o = 8 s and t_r = 4 s). SEM images and respective size distributions of Cu cubes synthesized with a 5 mM $CuSO_4$ solution mixed with a KCl solution of the following concentrations: (b) 0 mM KCl (1:0, no Cl^-), (c) 5 mM KCl (1:1), (d) 10 mM KCl (1:2), (e) 30 mM KCl (1:6), and (f) 50 mM KCl (1:10). In (g) 50 mM $CuSO_4$ + 5 mM KCl (10:1) were used to see the effect of further increasing the $CuSO_4$ concentration. The respective current response can be seen in Figure S1.

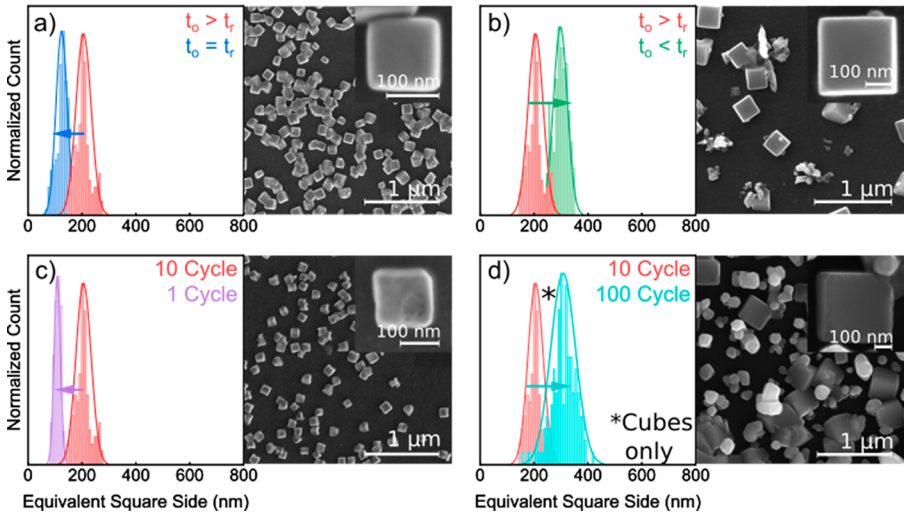

Figure 2. Effect of varying the time length and number of cycles of the synthesis protocol with constant precursor concentrations (5 mM $CuSO_4$ and 5 mM KCl). Different times for t_r and t_o with (a) $t_r = t_o$ and (b) $t_r > t_o$ as well as change in the number of cycles with (c) 1 cycle and (d) 100 cycles compared to the $t_r < t_o$, 10 cycle reference.

Because during the electrodeposition process the growth speed is governed by the availability of ionic metal species (M^+),

https://dx.doi.org/10.1021/acs.jpcc.0c09105
J. Phys. Chem. C 2020, 124, 26908−26915

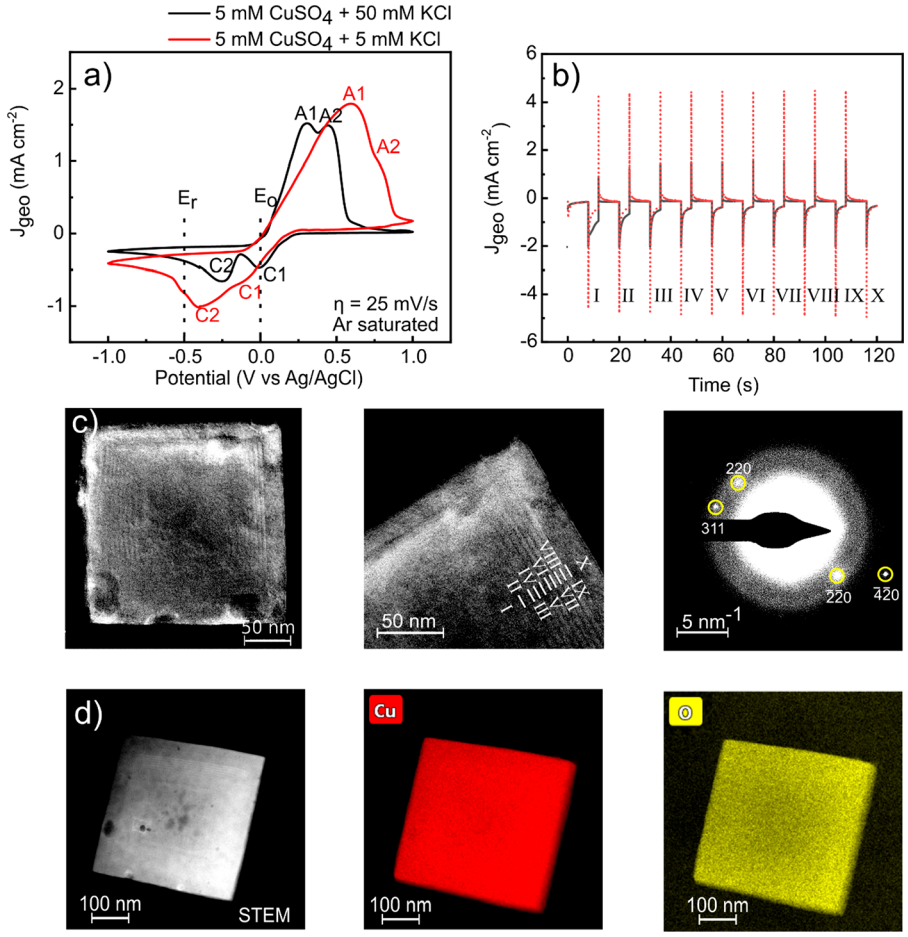

Figure 3. (a) Cyclic voltammograms (CV) in 5 mM $CuSO_4$ and 5 mM KCl/50 mM KCl at 25 mV s^{-1} to show the current response at the potentials E_r and E_o. The anodic peaks A1 and A2 represent the oxidation to Cu_2O and CuO, and the cathodic peaks are typically interpreted as the corresponding reductive counterparts.[50] In (b), the current responses for 1:1 and 1:10 Cu-to-Cl ratio samples (t_r = 4 s, t_o = 8 s, 10 cycles labeled I–X) at the potentials E_r and E_o are shown. TEM images and electron diffraction patterns of 1:1 cubes prepared with the same procedure are shown in (c), with the Roman numbers indicating layers correlated to the respective cycle in (b). The colors are inverted for better visibility. In (d), the EDX mapping of the same pristine Cu cubes on the carbon working electrode of the liquid cell chips used for TEM are shown.

which is given by the concentration of the metal salt in solution, we have kept this parameter constant (5 mM $CuSO_4$) for a more direct comparison of the role of other parameters.

Figure 1 shows how the morphology of electrodeposited particles, obtained from SEM, varies as a function of the Cl^- concentration from 5 to 50 mM, leading to different Cu-to-Cl ratios in the precursor solution. The alternating potential cycles used for the electrodeposition are depicted in Figure 1a. Figure 1b shows that such protocol can still yield cubelike structures without the presence of Cl^- ions in solution but that their average size is much larger and exhibits a broader size distribution as compared to the samples where Cl^- was added. Moreover, the cube corners are truncated. Figures 1c–f show that with increasing concentration of Cl^- and constant Cu^+ concentration (5 mM $CuSO_4$) cubes with sharp corners are obtained, and the cube size was found to decrease while the surface density of the cubes on the support increased. At a Cu-to-Cl ratio of 1:6 (5 mM $CuSO_4$ to 30 mM KCl), the cubes start to interconnect as shown in Figure 1e. Furthermore, the cube coverage is the highest for this Cu/Cl ratio. For a KCl concentration of 50 mM, the cubes no longer maintain a sharp cubic shape and the corners start to become rounded (Figure 1f). Increasing the concentration of $CuSO_4$ to 50 mM, while keeping the KCl concentration at 5 mM KCl (10:1) (Figure 1g), leads to a significant change in the deposited morphology, with large micrometer-sized branched structures. A closer examination of these flowerlike structures further suggest that they are made up of merged cubes (inset in Figure 1g).

On the basis of the size distributions, we calculated the exposed electrochemical Cu surface (specific $area_{(Cu\text{-}cubes)}$) assuming a cubic geometry. The results are summarized in Table 1. For all Cl^--containing samples synthesized under identical conditions, the exposed surface area of Cu is similar, while without the addition of Cl^-, the surface area is significantly smaller. This estimation does not account for the loss of exposed facets due to the interconnection of the cubes; thus, it may lead to an overestimation of the surface area for those samples.

In Figure 2, we summarize the effect that changing the duration of the applied reductive potential (E_r), oxidative potential (E_o), and the number of applied cycles have on the morphology. Previously, we had shown with *in situ* TEM that noncubic particles dissolve earlier than the cubic ones during the oxidative part of the cycle.[47] By cycling repetitively within a potential window where the noncubic particles dissolve and the cubic ones do not, we could induce selection toward cubic shapes. Now, we use Figure 1c as the reference point for comparison (5 mM $CuSO_4$ and 5 mM KCl) with 10 alternating potential cycles of t_o = 8 s and t_r = 4 s. Our results indicate that a

https://dx.doi.org/10.1021/acs.jpcc.0c09105
J. Phys. Chem. C 2020, 124, 26908–26915

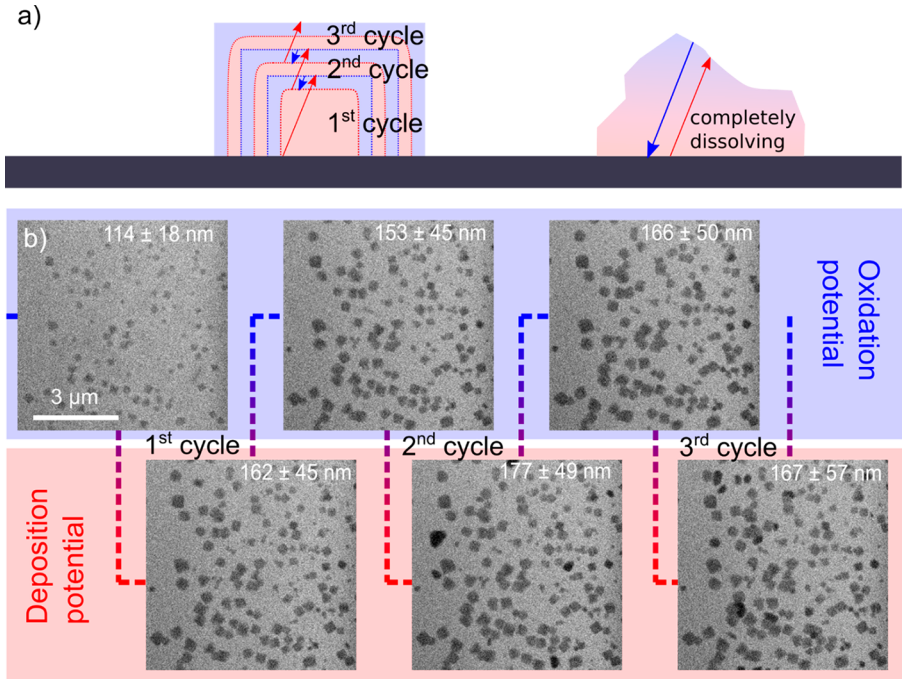

Figure 4. (a) Scheme of the proposed mechanism for the growth of Cu cubes by electrodeposition, with layer growth during E_r and shrinkage during E_o. The noncubic particles dissolve completely after growth during E_r. (b) *Operando* SEM images of the second to fourth electrochemical cycles in a 5 mM $CuSO_4$ + 5 mM KCl solution synthesized by the electrochemical protocol discussed in Figure 3.

longer oxidative potential is preferred to dissolve noncubic particles completely.[47] An increase in the reductive potential results in larger cubes, but it comes at the expense of the growth of noncubic particles that do not fully dissolve during the oxidative potential. In Figure 2a, we show that applying the same duration for both the oxidative and the reductive potential (t_r = t_o = 4 s) surprisingly leads to smaller cubes (roughly half the size of those shown in Figure 1c) with triple surface coverage. The calculated specific area of Cu is in this case approximately two-thirds of that of the 1:1 sample with t_o = 8 s shown in Figure 1c. If t_r is longer than t_o, the size distribution shifts to larger cube sizes together with the formation of branched structures (Figure 2b). Additionally, the specific area of the Cu cubic particles is reduced to approximately one-third. The size distribution and surface area calculation results, normalized to 1 cm^2 sample size, are summarized in Table 2.

Lastly, we varied the number of cycles while using the same cycling parameters as in Figure 1c of t_o = 8 s and t_r = 4 s. From Figure 2c, we can see that applying only a single oxidative−reductive potential cycle leads to the formation of smaller, but poorly shaped cubes, suggesting that these are the initial nuclei from which the larger cubes are formed in the subsequent cycles. On the other hand, increasing the number of cycles to 100 (Figure 2d) leads to a densely covered surface, but with significant dispersion in terms of both particle size and shape.

For a better understanding of the parameters that enable a high surface coverage of size- and shape-controlled Cu_2O cubes, we further examined the electrochemical characteristics of the deposition process using cyclic voltammetry (CV) and the deposited structures using electron microscopy. Figure 3a compares the CV curves of a glassy carbon support in a solution of 5 mM $CuSO_4$ and 5 mM KCl as well as a second solution with 50 mM KCl, both in Ar-saturated ultrapure water. In our protocol for the electrodeposition we alternated between two potentials, a reductive potential (E_r) at −0.5 V vs Ag/AgCl and a slightly oxidative potential (E_o) at +0.0 V vs Ag/AgCl, indicated by the dotted lines in Figure 3a. E_r lies at a potential higher than the maximum of the two cathodic peaks, and E_o lies at the onset of the anodic peaks. With increasing concentration of Cl^- (and K^+) ions the conductivity increases, which reduces the distance between the cathodic and anodic peaks A1/2 and C1/2, respectively. Hence, changing the Cl^- concentration also resulted in modifications of the deposition and dissolution currents and, thereby, in changes in the growth rate of the cubes. As shown in Figure 3b, the deposition and dissolution currents in the 50 mM KCl cycling experiment are about 4 times larger than those in the 5 mM KCl experiment.

Figure 3c shows high-resolution TEM images and the selected area electron diffraction (SAED) pattern of a 1:1 Cu-to-Cl ratio sample obtained by depositing the cubes directly on the carbon working electrode of the liquid cell chips used in the *in situ* SEM experiments described later in this article. Figure 3d shows the corresponding scanning TEM (STEM) image and energy-dispersive X-ray (EDX) spectroscopy map of a cube. The TEM and STEM images indicate that we form solid cubes with small pores near the surface. The SAED pattern shows that the cube is a Cu_2O single crystal. The strong diffraction spots at the (311) and (−4−20) positions together with diffuse spots at (220) and (−2−20) are consistent with the pattern of a tilted crystal which is not orientated close to a zone axis. A closer inspection of the image also reveals subtle layering in the internal structure of the cube (second panel in Figure 3c). The STEM image provides more detail regarding the structure, where one can distinguish a slightly porous cubic core with uniform contrast, followed by alternating layers of brighter and darker contrast, before ending with a thicker layer of darker contrast. These changes in contrast are likely caused by small changes in the density between an oxidized layer and the subsequently deposited layer.

These results, together with the poorly formed cubes after a single deposition cycle that is shown in Figure 2c, suggest a cube

https://dx.doi.org/10.1021/acs.jpcc.0c09105
J. Phys. Chem. C 2020, 124, 26908−26915

growth pathway where the poorly formed cube serves as nuclei for subsequent growth. The thickness of the final surface layer indicates that the reductive part of the cycle actually increases the thickness of the cube by a substantial amount, which is then removed to a larger degree during the oxidative part of the cycle, leaving behind only a portion of the deposited layer. The last layer is thicker because the applied protocol ends at the reductive potential. This mechanism is summarized as a schematic in Figure 4a.

To confirm this growth mechanism, we acquired electrochemical SEM images to follow the nucleation and growth of the particles during potential cycling. Images extracted from the first three cycles of the *in situ* image sequence are shown in Figure 4b, and the full movie sequence covering 11 cycles is provided as Movie S1. Consistent with the proposed mechanism, we only observe small, partially developed cubic structures with truncated corners and broken edges during the first cycle (enlarged image in Figure S2). The nucleation process itself was not possible to observe due to limitations in the microscope resolution.

The *in situ* image sequence revealed that the cubes are nearly fully formed by the end of the third cycle. Furthermore, we were able to see the dynamic formation and dissolution of noncubic particles during each potential cycle, as we reported previously via TEM.[47] A comparison of the images acquired at the second and fourth deposition cycles also indicates that ~80% of the final cubic structures were formed from the initial semicubic nanostructures. We could measure a slight increase ~5−10% in size with each deposition step, corroborating our proposed mechanism.

On the basis of these results, we can rationalize why our standard protocol appears to be optimal for generating size- and shape-controlled Cu_2O cubes and provide general principles for modifying the protocol to achieve tuning of the cube morphology. First, it is clear that the Cl^- ion concentration influences both the nucleation of the Cu_2O cubes and the stabilization of the cubic shape. It is known that both Cl^- and SO_4^- ions can act as modifiers to stabilize specific crystal orientations.[51] Cl^- ions stabilize the Cu{100} facet, whereas SO_4^- ions stabilize both Cu{111} and Cu{100} facets. Hence, the formation of truncated cubes in the absence of Cl^- can be easily attributed to the effect of SO_4^-. When KCl is however added, the effect of chloride dominates due to stronger adsorption of Cl^- ions to the Cu surface.[51]

The increased coverage of cubes on the glassy carbon surface and the reduction in size of the cubes are, on the other hand, attributed to the increased conductivity of the electrolyte due to the added KCl and the relatively low concentrations of $CuSO_4$ used in our deposition solutions. The higher deposition currents at higher KCl concentrations lead to the formation of more $CuSO_4$ nuclei, as indicated by the increasing density of cubes on the support surface with increasing KCl concentration. Presumably, the higher cube density also aggravated the local depletion of Cu^{2+} during the reduction cycle, resulting in a reduced growth and smaller initial cube sizes. We note here that this trend is not sustained at the highest Cu:Cl ratio of 1:10, where we also start to see poorly formed cubic structures, suggesting that at 50 mM KCl, the nucleated cubes start to be etched from the support surface by the high dissolution currents present during the oxidative cycles. Within these limits, the final size distribution can be then tuned by adjusting the durations of t_o and t_r and the number of cycles. Increasing the number of cycles by a significant amount, however, appears to have a detrimental effect on the monodispersity of the deposited catalysts (Figure 2d). This is likely due to the increase in the probability of the new nuclei formation with additional cycles.[47]

It is also interesting that increasing the $CuSO_4$ concentration to 50 mM does not cause an increased coverage of the support surface by Cu structures. Instead, it causes branching of the initial cubes, as seen in Figure 1f. A significant increase of branching has been reported for electrodeposition at high currents or high potentials.[52] In this case, the branching can be attributed to either the mass transport arguments that correlate the Cu concentration to the surface free energy of the particles previously put forth by Radi et al.[53] or the overpotential induced concentration gradients proposed by Siegfried and Choi.[54]

CONCLUSION

In this work, we explore the synthesis parameters governing the electrodeposition of size- and shape-controlled cubic Cu_2O structures for catalytic applications. We found that the concentration of Cl^- ions in solution controls the formation of cubic shapes, the cube size, the initial coverage, and the dispersion of the cubes on the support. The ratio of reductive and oxidative times in our alternating potential electrodeposition protocol can be used to tune the coverage of the Cu catalysts on the support surface, whereas the number of cycles determines the size of the cubes and monodispersity. The mechanisms responsible for the Cu cube growth are further investigated by using *ex situ* and *in situ* electron microscopy, featuring the importance of applying successive cycles. These results reveal the role of the alternating potential cycles in controlling the cube growth. In particular, after the Cu nuclei are formed during the first deposition cycle, new layers of material are progressively added and then partially removed in subsequent cycles. The principles described here provide guidelines for obtaining and controlling the growth of monodisperse cubic Cu_2O catalysts.

ASSOCIATED CONTENT

Supporting Information

The Supporting Information is available free of charge at https://pubs.acs.org/doi/10.1021/acs.jpcc.0c09105.

Synthesis current response plots; first cycle cube shape images (PDF)

Operando liquid phase electron microscopy video (AVI)

AUTHOR INFORMATION

Corresponding Author

Beatriz Roldan Cuenya − *Department of Interface Science, Fritz-Haber Institute of the Max Planck Society, 14195 Berlin, Germany*; orcid.org/0000-0002-8025-307X; Email: Roldan@fhi-berlin.mpg.de

Authors

Philipp Grosse − *Department of Interface Science, Fritz-Haber Institute of the Max Planck Society, 14195 Berlin, Germany*

Aram Yoon − *Department of Interface Science, Fritz-Haber Institute of the Max Planck Society, 14195 Berlin, Germany*

Clara Rettenmaier − *Department of Interface Science, Fritz-Haber Institute of the Max Planck Society, 14195 Berlin, Germany*

See Wee Chee − *Department of Interface Science, Fritz-Haber Institute of the Max Planck Society, 14195 Berlin, Germany*

Complete contact information is available at:

https://dx.doi.org/10.1021/acs.jpcc.0c09105
J. Phys. Chem. C 2020, 124, 26908−26915

https://pubs.acs.org/10.1021/acs.jpcc.0c09105

Notes

The authors declare no competing financial interest.

■ ACKNOWLEDGMENTS

Financial support for this work was provided the European Research Council under Grant ERC-OPERANDOCAT (ERC-725915) and the Deutsche Forschungsgemeinschaft (DFG, German Research Foundation) under Germany's Excellence Strategy - EXC 2008/1 (UniSysCat) - 390540038 and the SFB 1316, project no. 327886311, subproject B1.

■ REFERENCES

(1) De Luna, P.; Hahn, C.; Higgins, D.; Jaffer, S. A.; Jaramillo, T. F.; Sargent, E. H. What Would It Take for Renewably Powered Electrosynthesis to Displace Petrochemical Processes? *Science* **2019**, *364* (6438), eaav3506.

(2) Nitopi, S.; Bertheussen, E.; Scott, S. B.; Liu, X.; Engstfeld, A. K.; Horch, S.; Seger, B.; Stephens, I. E.; Chan, K.; Hahn, C.; et al. Progress and Perspectives of Electrochemical CO_2 Reduction on Copper in Aqueous Electrolyte; *Chem. Rev.* **2019**, *119*, 7610−7672.

(3) Ross, M. B.; De Luna, P.; Li, Y.; Dinh, C. T.; Kim, D.; Yang, P.; Sargent, E. H. Designing Materials for Electrochemical Carbon Dioxide Recycling. *Nat. Catal.* **2019**, *2* (8), 648−658.

(4) Luo, F.; Roy, A.; Silvioli, L.; Cullen, D. A.; Zitolo, A.; Sougrati, M. T.; Oguz, I. C.; Mineva, T.; Teschner, D.; Wagner, S.; et al. P-Block Single-Metal-Site Tin/Nitrogen-Doped Carbon Fuel Cell Cathode Catalyst for Oxygen Reduction Reaction. *Nat. Mater.* **2020**, *19*, 1215−1223.

(5) Jiao, Y.; Zheng, Y.; Davey, K.; Qiao, S. Z. Activity Origin and Catalyst Design Principles for Electrocatalytic Hydrogen Evolution on Heteroatom-Doped Graphene. *Nat. Energy* **2016**, *1* (10), 1−9.

(6) Lin, Y. X.; Zhang, S. N.; Xue, Z. H.; Zhang, J. J.; Su, H.; Zhao, T. J.; Zhai, G. Y.; Li, X. H.; Antonietti, M.; Chen, J. S. Boosting Selective Nitrogen Reduction to Ammonia on Electron-Deficient Copper Nanoparticles. *Nat. Commun.* **2019**, *10* (1), 1−7.

(7) Kang, U.; Yoon, S. H.; Han, D. S.; Park, H. Synthesis of Aliphatic Acids from CO_2 and Water at Efficiencies Close to the Photosynthesis Limit Using Mixed Copper and Iron Oxide Films. *ACS Energy Lett.* **2019**, *4* (9), 2075−2080.

(8) Aljaafari, A.; Parveen, N.; Ahmad, F.; Alam, M. W.; Ansari, S. A. Self-Assembled Cube-like Copper Oxide Derived from a Metal-Organic Framework as a High-Performance Electrochemical Supercapacitive Electrode Material; *Sci. Rep.* **2019**, *9*, 1−10.

(9) Kas, R.; Kortlever, R.; Yilmaz, H.; Koper, M. T. M.; Mul, G. Manipulating the Hydrocarbon Selectivity of Copper Nanoparticles in CO_2 Electroreduction by Process Conditions. *ChemElectroChem.* **2015**, *2* (3), 354−358.

(10) Li, C. W.; Kanan, M. W. CO_2 Reduction at Low Overpotential on Cu Electrodes Resulting from the Reduction of Thick Cu_2O Films. *J. Am. Chem. Soc.* **2012**, *134* (17), 7231−7234.

(11) Appel, A. M. Electrochemistry: Catalysis at the Boundaries. *Nature* **2014**, *508* (7497), 460−461.

(12) Roberts, F. S.; Kuhl, K. P.; Nilsson, A. High Selectivity for Ethylene from Carbon Dioxide Reduction over Copper Nanocube Electrocatalysts. *Angew. Chem., Int. Ed.* **2015**, *54* (17), 5179−5182.

(13) Loiudice, A.; Lobaccaro, P.; Kamali, E. A. A.; Thao, T.; Huang, B. H. H.; Ager, J. W. W.; Buonsanti, R. Tailoring Copper Nanocrystals towards C2 Products in Electrochemical CO_2 Reduction. *Angew. Chem., Int. Ed.* **2016**, *55* (19), 5789−5792.

(14) Schouten, K. J. P.; Pérez Gallent, E.; Koper, M. T. M. Structure Sensitivity of the Electrochemical Reduction of Carbon Monoxide on Copper Single Crystals. *ACS Catal.* **2013**, *3* (6), 1292−1295.

(15) Calle-Vallejo, F.; Koper, M. T. M. M. Theoretical Considerations on the Electroreduction of CO to C2 Species on Cu(100) Electrodes. *Angew. Chem.* **2013**, *125* (28), 7423−7426.

(16) Montoya, J. H.; Shi, C.; Chan, K.; Nørskov, J. K. Theoretical Insights into a CO Dimerization Mechanism in CO_2 Electroreduction. *J. Phys. Chem. Lett.* **2015**, *6* (11), 2032−2037.

(17) Kim, D.; Kley, C. S.; Li, Y.; Yang, P. Copper Nanoparticle Ensembles for Selective Electroreduction of CO_2 to C2-C3 Products. *Proc. Natl. Acad. Sci. U. S. A.* **2017**, *114* (40), 10560−10565.

(18) Tang, W.; Peterson, A. A.; Varela, A. S.; Jovanov, Z. P.; Bech, L.; Durand, W. J.; Dahl, S.; Nørskov, J. K.; Chorkendorff, I. The Importance of Surface Morphology in Controlling the Selectivity of Polycrystalline Copper for CO_2 Electroreduction. *Phys. Chem. Chem. Phys.* **2012**, *14* (1), 76−81.

(19) Sandberg, R. B.; Montoya, J. H.; Chan, K.; Nørskov, J. K. CO-CO Coupling on Cu Facets: Coverage, Strain and Field Effects. *Surf. Sci.* **2016**, *654*, 56−62.

(20) Zegkinoglou, I.; Zendegani, A.; Sinev, I.; Kunze, S.; Mistry, H.; Jeon, H. S.; Zhao, J.; Hu, M. Y.; Alp, E. E.; Piontek, S.; et al. Operando Phonon Studies of the Protonation Mechanism in Highly Active Hydrogen Evolution Reaction Pentlandite Catalysts. *J. Am. Chem. Soc.* **2017**, *139* (41), 14360−14363.

(21) Todorova, T. K.; Schreiber, M. W.; Fontecave, M. Mechanistic Understanding of CO_2 Reduction Reaction (CO_2RR) Toward Multicarbon Products by Heterogeneous Copper-Based Catalysts. *ACS Catal.* **2020**, *10* (3), 1754−1768.

(22) De Luna, P.; Quintero-Bermudez, R.; Dinh, C. T.; Ross, M. B.; Bushuyev, O. S.; Todorović, P.; Regier, T.; Kelley, S. O.; Yang, P.; Sargent, E. H. Catalyst Electro-Redeposition Controls Morphology and Oxidation State for Selective Carbon Dioxide Reduction. *Nat. Catal.* **2018**, *1* (2), 103−110.

(23) Grosse, P.; Gao, D.; Scholten, F.; Sinev, I.; Mistry, H.; Roldan Cuenya, B. Dynamic Changes in the Structure, Chemical State and Catalytic Selectivity of Cu Nanocubes during CO_2 Electroreduction: Size and Support Effects. *Angew. Chem., Int. Ed.* **2018**, *57* (21), 6192−6197.

(24) Mistry, H.; Varela, A. S.; Kühl, S.; Strasser, P.; Cuenya, B. R. Nanostructured Electrocatalysts with Tunable Activity and Selectivity. *Nat. Rev. Mater.* **2016**, *1* (4), 16009.

(25) Kortlever, R.; Shen, J.; Schouten, K. J. P.; Calle-Vallejo, F.; Koper, M. T. M. Catalysts and Reaction Pathways for the Electrochemical Reduction of Carbon Dioxide. *J. Phys. Chem. Lett.* **2015**, *6* (20), 4073−4082.

(26) Larrazábal, G. O.; Martín, A. J.; Pérez-Ramírez, J. Building Blocks for High Performance in Electrocatalytic CO_2 Reduction: Materials, Optimization Strategies, and Device Engineering. *J. Phys. Chem. Lett.* **2017**, *8* (16), 3933−3944.

(27) Mistry, H.; Varela, A. S.; Bonifacio, C. S.; Zegkinoglou, I.; Sinev, I.; Choi, Y.-W.; Kisslinger, K.; Stach, E. A.; Yang, J. C.; Strasser, P.; Cuenya, B. R.; et al. Highly Selective Plasma-Activated Copper Catalysts for Carbon Dioxide Reduction to Ethylene. *Nat. Commun.* **2016**, *7*, 12123.

(28) Gao, D.; Zegkinoglou, I.; Divins, N. J.; Scholten, F.; Sinev, I.; Grosse, P.; Roldan Cuenya, B. Plasma-Activated Copper Nanocube Catalysts for Efficient Carbon Dioxide Electroreduction to Hydrocarbons and Alcohols. *ACS Nano* **2017**, *11* (5), 4825−4831.

(29) Gao, D.; Scholten, F.; Roldan Cuenya, B. Improved CO_2 Electroreduction Performance on Plasma-Activated Cu Catalysts via Electrolyte Design: Halide Effect. *ACS Catal.* **2017**, *7* (8), 5112−5120.

(30) Reller, C.; Krause, R.; Volkova, E.; Schmid, B.; Neubauer, S.; Rucki, A.; Schuster, M.; Schmid, G. Selective Electroreduction of CO_2 toward Ethylene on Nano Dendritic Copper Catalysts at High Current Density. *Adv. Energy Mater.* **2017**, *7* (12), 1602114.

(31) Eilert, A.; Cavalca, F.; Roberts, F. S.; Osterwalder, J.; Liu, C.; Favaro, M.; Crumlin, E. J.; Ogasawara, H.; Friebel, D.; Pettersson, L. G.; et al. Subsurface Oxygen in Oxide-Derived Copper Electrocatalysts for Carbon Dioxide Reduction. *J. Phys. Chem. Lett.* **2017**, *8* (1), 285−290.

(32) Lee, S.; Kim, D.; Lee, J. Electrocatalytic Production of C3-C4 Compounds by Conversion of CO_2 on a Chloride-Induced Bi-Phasic Cu_2O-Cu Catalyst. *Angew. Chem., Int. Ed.* **2015**, *54* (49), 14701−14705.

https://dx.doi.org/10.1021/acs.jpcc.0c09105
J. Phys. Chem. C 2020, 124, 26908−26915

(33) Ren, D.; Deng, Y.; Handoko, A. D.; Chen, C. S.; Malkhandi, S.; Yeo, B. S. Selective Electrochemical Reduction of Carbon Dioxide to Ethylene and Ethanol on Copper(I) Oxide Catalysts. *ACS Catal.* **2015**, *5* (5), 2814−2821.
(34) Xiao, H.; Goddard, W. A.; Cheng, T.; Liu, Y. Cu Metal Embedded in Oxidized Matrix Catalyst to Promote CO_2 Activation and CO Dimerization for Electrochemical Reduction of CO_2. *Proc. Natl. Acad. Sci. U. S. A.* **2017**, *114* (26), 6685−6688.
(35) Favaro, M.; Xiao, H.; Cheng, T.; Goddard, W. A.; Yano, J.; Crumlin, E. J. Subsurface Oxide Plays a Critical Role in CO_2 Activation by Cu(111) Surfaces to Form Chemisorbed CO_2, the First Step in Reduction of CO_2. *Proc. Natl. Acad. Sci. U. S. A.* **2017**, *114* (26), 6706−6711.
(36) Wang, X.; Varela, A. S.; Bergmann, A.; Kühl, S.; Strasser, P. Catalyst Particle Density Controls Hydrocarbon Product Selectivity in CO_2 Electroreduction on CuO_x. *ChemSusChem* **2017**, *10* (22), 4642−4649.
(37) Hori, Y.; Takahashi, I.; Koga, O.; Hoshi, N. Electrochemical Reduction of Carbon Dioxide at Various Series of Copper Single Crystal Electrodes. *J. Mol. Catal. A: Chem.* **2003**, *199* (1−2), 39−47.
(38) Todorova, T. K.; Schreiber, M. W.; Fontecave, M. Mechanistic Understanding of CO_2 Reduction Reaction (CO_2RR) Toward Multicarbon Products by Heterogeneous Copper-Based Catalysts. *ACS Catal.* **2020**, *10*, 1754−1768.
(39) Pérez-Gallent, E.; Figueiredo, M. C.; Calle-Vallejo, F.; Koper, M. T. M. M. Spectroscopic Observation of a Hydrogenated CO Dimer Intermediate During CO Reduction on Cu(100) Electrodes. *Angew. Chem., Int. Ed.* **2017**, *56* (13), 3621−3624.
(40) Li, H.; Li, Y.; Koper, M. T. M. M.; Calle-Vallejo, F. Bond-Making and Breaking between Carbon, Nitrogen, and Oxygen in Electrocatalysis. *J. Am. Chem. Soc.* **2014**, *136* (44), 15694−15701.
(41) Tanori, J.; Pileni, M. P. Control of the Shape of Copper Metallic Particles by Using a Colloidal System as Template. *Langmuir* **1997**, *13* (4), 639−645.
(42) Feng, Y.; Li, Z.; Liu, H.; Dong, C.; Wang, J.; Kulinich, S. A.; Du, X. Laser-Prepared CuZn Alloy Catalyst for Selective Electrochemical Reduction of CO_2 to Ethylene. *Langmuir* **2018**, *34* (45), 13544−13549.
(43) Liu, D.; Fernández, Y.; Ola, O.; MacKintosh, S.; Maroto-Valer, M.; Parlett, C. M. A.; Lee, A. F.; Wu, J. C. S. On the Impact of Cu Dispersion on CO_2 Photoreduction over Cu/TiO_2. *Catal. Commun.* **2012**, *25*, 78−82.
(44) Wang, Z.; Liu, Q.; Yu, J.; Wu, T.; Wang, G. Surface Structure and Catalytic Behavior of Silica-Supported Copper Catalysts Prepared by Impregnation and Sol-Gel Methods. *Appl. Catal., A* **2003**, *239* (1−2), 87−94.
(45) Potochnik, S. J.; Pehrsson, P. E.; Hsu, D. S. Y.; Calvert, J. M. Selective Copper Chemical Vapor Deposition Using Pd-Activated Organosilane Films. *Langmuir* **1995**, *11* (6), 1841−1845.
(46) Eilert, A.; Roberts, F. S.; Friebel, D.; Nilsson, A. Formation of Copper Catalysts for CO_2 Reduction with High Ethylene/Methane Product Ratio Investigated with in Situ X-Ray Absorption Spectroscopy. *J. Phys. Chem. Lett.* **2016**, *7* (8), 1466−1470.
(47) Aran-Ais, R. M.; Rizo, R.; Grosse, P.; Algara-Siller, G.; Dembele, K.; Plodinec, M.; Lunkenbein, T.; Chee, S. W.; Cuenya, B. R. Imaging Electrochemically Synthesized Cu_2O Cubes and Their Morphological Evolution under Conditions Relevant to CO_2 Electroreduction. *Nat. Commun.* **2020**.
(48) Varela, A. S.; Ju, W.; Reier, T.; Strasser, P. Tuning the Catalytic Activity and Selectivity of Cu for CO_2 Electroreduction in the Presence of Halides. *ACS Catal.* **2016**, *6* (4), 2136−2144.
(49) Krasnikov, G. Y.; Bokarev, V. P. Surface Energy and Crystal Faceting of Elemental Semiconductors and Other Substances. *Dokl. Phys. Chem.* **2002**, *382* (1−3), 14−17.
(50) Velasco-Vélez, J. J.; Skorupska, K.; Frei, E.; Huang, Y. C.; Dong, C. L.; Su, B. J.; Hsu, C. J.; Chou, H. Y.; Chen, J. M.; Strasser, P.; et al. The Electro-Deposition/Dissolution of $CuSO_4$ Aqueous Electrolyte Investigated by In Situ Soft X-Ray Absorption Spectroscopy. *J. Phys. Chem. B* **2018**, *122* (2), 780−7.
(51) Siegfried, M. J. J.; Choi, K.-S. S. Elucidating the Effect of Additives on the Growth and Stability of Cu 2O Surfaces via Shape Transformation of Pre-Grown Crystals. *J. Am. Chem. Soc.* **2006**, *128* (32), 10356−10357.
(52) Siegfried, M. J.; Choi, K.-S. Directing the Architecture of Cuprous Oxide Crystals during Electrochemical Growth. *Angew. Chem.* **2005**, *117* (21), 3282−3287.
(53) Radi, A.; Pradhan, D.; Sohn, Y.; Leung, K. T. Nanoscale shape and size control of cubic, cuboctahedral, and octahedral Cu-Cu_2O core-shell nanoparticles on Si(100) by one-step, templateless, capping-agent-free electrodeposition. *ACS Nano* **2010**, *4* (3), 1553−1560.
(54) Siegfried, M. J.; Choi, K. S. Elucidation of an Overpotential-Limited Branching Phenomenon Observed during the Electrocrystallization of Cuprous Oxide. *Angew. Chem., Int. Ed.* **2008**, *47* (2), 368−372.

https://dx.doi.org/10.1021/acs.jpcc.0c09105
J. Phys. Chem. C 2020, 124, 26908−26915